Influence of Grain Size on the Constitutive Response and Substructure Evolution of MONEL 400

GEORGE T. GRAY III, SHUH RONG CHEN, and KENNETH S. VECCHIO

The influence of grain size on the constitutive behavior (strain-rate and temperature dependence of the yield stress and strain hardening) and substructure evolution of MONEL 400 was investigated. Increasing the grain size from 9.5 to 202 μm was seen to reduce the quasi-static yield strength from 290 to 115 MPa, while having a minimal effect on the work-hardening response. Increasing the strain rate from quasi-static to dynamic strain rates (3000 s^{-1}) was seen to increase the yield and overall flow-stress levels, but has no effect on the strong grain-size dependency exhibited by this alloy. The persistent influence of grain size to large strains is inconsistent with previous $d^{-1/2}$ pileup grain-size modeling in the literature, which predicts convergence at large strains. Substructure evolution differences between the grain interiors and adjacent to grain boundaries supports differential defect storage processes which are consistent with previously published work-hardening d^{-1} modeling arguments for grain size–dependent strengthening in polycrystals. The integration of grain-size dependency into constitutive modeling using the mechanical threshold stress (MTS) model is discussed. The MTS model is shown to provide a robust constitutive description capturing yielding, large-strain work hardening, and grain-size effects simultaneously. The MTS model is, additionally, shown to satisfactorily address the experimentally observed transients due to strain-rate or temperature-path dependency.

I. INTRODUCTION

THE strength of polycrystalline metals and alloys is well documented to increase with decreasing grain size. This strengthening effect has been empirically shown to follow the linear relation

$$\sigma = M(\sigma_0 + k_y \cdot d^{-n}) \qquad [1]$$

where σ is either the yield stress or flow stress at a fixed strain, σ_0 is referred to as a friction stress, d is the grain diameter, k_y is the "unpinning constant" at the yield point (similarly, k_f is used when referring to the unpinning value at some finite plastic strain), and M is the Taylor orientation factor. The terms σ_0, k_y, k_f, M, and n are material-dependent constants. The parameter k_y was originally considered to be a measure of the stress required at the tip of a dislocation pileup to unlock pinned dislocations[1] or to create new dislocations in the adjacent grain;[2] later analysis,[2] as described subsequently, suggests that it reflects the stress necessary to cause a dislocation emission from a boundary or source. Physically, this reflects the resistance of grain or phase boundaries to the spread of slip bands.[1,3–8] This strengthening relationship, with $n = 1/2$, was formulated to account for the grain-size dependency of the yield strength of mild steels by Hall[9] and Petch.[10] Over the past 40 years, this equation, referred to as the "Hall–Petch equation," has been used to correlate a wide range of grain-size (or microstructural-unit size, *i.e.*, cell-size, subgrain, *etc.*) *vs* yield or flow-stress data.

Hall–Petch relationships have been shown, in several reviews, to correlate with a number of additional mechanical properties, including indentation hardness, tensile ductile-to-brittle transition temperature, fatigue-limit strength, fatigue-crack growth resistance, and polycrystalline creep rate.[1–3,11–13] In many of these cases, the $n = 1/2$ power relation has been verified over a wide range of grain sizes, and the dependency of yield strength on grain size can be significant for many materials, while, in other materials, grain-size effects on yielding are quite modest. Typical values for the material parameters σ_0 and k_y, for a large number of metals and alloys, including some ordered intermetallics, have been summarized by Hall.[1] The range in effects of grain size on yield or flow stress at small strains is given in Table I for several materials. Although alternative relationships to $n = 1/2$ (*i.e.*, n values ranging from 1/3 to 1) have been offered by several authors, including Baldwin,[14] Kocks,[15] Conrad,[16] Anderson *et al.*,[17] and Mecking,[18] the $n = 1/2$ dependency has been found to be widely applicable to steels, as well as to a large number of other metals and alloys.[1]

Several in-depth review articles have summarized the effects of externally imposed constraints and microstructural variables, such as stress state, temperature, strain rate, *etc.*, on the parameters in the Hall–Petch relation.[1,2,3] Changes in the propensity for a material to cross-slip, *via* either structural ordering or decreases in stacking-fault energy, have been shown to increase the Hall–Petch slope due to a reduction of the number of active slip systems.[1,19] In mild steels, k_y is relatively composition insensitive,[1,3] while, in copper-based alloys,[20] k_y is seen to increase substantially with increased alloying. Variations in strain rate from 10^{-4} to 2350 s^{-1} were found to have no effect on the k_y term for the lower yield stress of pure iron tested at room temperature.[21] The k_y term for copper has been found to be independent of strain rate, over the range from 0.001 to 100 s^{-1}, as well as to strains of 0.20.[22]

While a number of models have been proposed to explain the dependence of plastic flow on grain size, two general

GEORGE T. GRAY III, Team Leader, Dynamic Properties, MST-8, and SHUH RONG CHEN, Technical Staff Member, are with the Los Alamos National Laboratory, Los Alamos, NM 87545. KENNETH S. VECCHIO, Professor, is with the Department of AMES, University of California-San Diego, La Jolla, CA 92093-0411.

Manuscript submitted January 26, 1998.

Table I. Typical Values of the Hall–Petch Terms σ_0 and k for Various Metals and Alloys[1]

Metal	Condition	σ_0 (MN/m^2)	k (MN/m$^{3/2}$)	$k/\mu\mathbf{b}^{1/2}$
Mild steel—0.06 pct C	lower yield point	41	0.66	0.655
Tantalum	yield point	124	0.31	0.299
Aluminum	flow stress at 0.5 pct ε	16	0.070	0.163
Copper	flow stress at 0.5 pct ε	26	0.12	0.178
Nickel	yield point	34	0.22	0.177
Cu-29Ni-29Zn	yield point	79	0.579	0.860*
Silver	flow stress at 0.5 pct ε	37	0.070	0.157
Titanium	yield point	79	0.41	0.548
Zirconium	flow stress at 0.2 pct ε	29	0.3	0.477

*The shear modulus and burgers vector for pure Cu were used in the absence of alloy data.

rationales have emerged: one based on dislocation pileups and the other based on dislocation-dislocation interactions through work hardening.[2] Although both dislocation pileups and dislocation-dislocation interactions might be expected to depend on temperature, k_y has been found to be remarkably temperature independent. Utilizing the experimentally observed correlation that dislocation density is also an inverse function of grain size, a $d^{-1/2}$ correlation has also been derived for some materials.[2,8] Consideration of the differences in the athermal work-hardening behavior in a polycrystal, between the grain interior and directly adjacent to the grain boundary, has also been used as the basis for modeling grain-size effects on flow behavior.[2,18,23] Within this "composite grain" framework, grain-size effects are viewed as resulting from the storage of geometrically redundant dislocations, rather than those geometrically necessary. The grain interior is assumed to harden similar to a single crystal, while a grain-boundary layer is envisioned to harden inversely with dislocation redundancy. Linear superposition of these two hardening behaviors can be shown to yield a d^{-1} (*i.e.*, $n = 1$) grain-size dependence.[18] Alternately, the superposition may be viewed as a pileup mechanism,[24] where dislocations are assumed to be driven from the softer grain cores into the harder boundary layer *via* a dislocation pileup. Given this superposition, the stress will depend on the grain size *via* $d^{-1/2}$.

The effect of work hardening and the exact details of how substructure evolution in a given material affects Hall–Petch behavior remains poorly understood. The work-hardening approach to Hall–Petch, being based upon athermal hardening, suggests that the applicability of the Hall–Petch correlation should decrease with increasing plastic strain, particularly at very large strains. As the grain size increases, athermal hardening effects will become less influential, and the statistically stored dislocations within the grains will become increasingly important.[19] The hardening behavior then depends on the strength of obstacles developed during strain hardening relative to the magnitude of the critical stresses for the propagation of slip at the boundaries. On this basis, in materials where cross-slip is easy and dislocation-dislocation interactions control hardening, the dependency of the flow stress on grain size has been suggested to disappear after moderate plastic strains of perhaps 0.20 to 0.40.[18]

As dynamic recovery occurs, which is proposed to affect the boundary areas first due to a higher dislocation density in these regions, grain-size effects should become less pronounced as the strain-hardening rate decreases.[18] While experimental studies support the belief that fine-grained materials work-harden more rapidly than coarse-grained materials, the variation of k_f with strain suggests that the behavior is significantly more complex than a simple accumulation model.[1,19] Indeed, it appears more plausible that the observed Hall–Petch correlation with flow stress for a broad range of materials, including both the initial yield behavior and the process of work hardening, is not consistent with a single controlling deformation mechanism. Rather, it may reflect an initial mechanism of slip transfer at or near boundaries, as well as the accumulation of dislocations due to grain compatibility constraints during continued straining.[19]

In addition to the scientific understanding of the Hall–Petch correlation, investigators have sought to incorporate grain-size dependencies into material-constitutive algorithms, such as those employed in three-dimensional (3-D) finite-element codes. [22,25–29] In the Johnson–Cook[25] and Zerilli–Armstrong[26] models, a term which incorporates the product of a "microstructural stress intensity-k" and the inverse square root of the average grain size have been added to the thermal stress. Gourdin and Lassila[22] also found that the grain-size dependency of the flow stress of copper was best described in the mechanical threshold stress (MTS) model[30] by adding a $k_y/(d^{1/2})$ component to the "athermal" stress term.

The purpose of this article is to report experimental observations and constitutive modeling results detailing the influence of grain size, strain rate, and temperature on the stress-strain response of MONEL* 400. The influence of grain size on the constitutive response is discussed in terms of (1) its ramifications on the physically based modeling concepts reviewed previously for explaining the Hall–Petch correlation, and (2) the manner by which grain size can be incorporated into constitutive-material models.

*MONEL is a trademark of Inco Alloys International Inc., Huntington, WV.

II. EXPERIMENTAL PROCEDURE

The material examined is the MONEL 400 alloy in the form of 9.5-mm-diameter hot-rolled wire. MONEL 400 is a solid solution–strengthened nickel-based alloy, whereby its hardening is achieved *via* mechanical working in addition to substitutional strengthening. The analyzed composition of the MONEL 400 wire is (in wt pct): 31.96 Cu, 2.1 Fe, 1.05 Mn, 0.11 Si, 0.05 Al, 0.03 C, 0.003 S, and 64.7 Ni. The as-rolled material has an equiaxed grain size of, nominally, 9.5 μm. To obtain a range of increasingly larger grain

Table II. Heat Treatment and Grain Sizes Used for MONEL 400

Heat Treatment	Grain Size (μm)
As-rolled (AR)	9.5 ± 0.4
AR + 1033 K/30 min	12 ± 0.8
AR + 1073 K/1 h	19 ± 0.7
AR + 1144 K/2 h	51 ± 1
AR + 1223 K/2 h	93 ± 2
AR + 1248 K/4 h	174 ± 6
AR + 1273 K/8 h	202 ± 5
AR + 1473 K/26 h	789 ± 11

sizes, samples were encapsulated in quartz tubes under vacuum and then annealed at various temperatures and times, followed by a slow bench cool, as given in Table II. The average grain size was measured by the linear-intercept method (14 lines, each 82 mm in length per photo) on a minimum of three micrographs taken at magnifications of 10, 50, 100, 200, or 500 times (the magnification chosen for each grain size to allow accurate measurement of the maximum number of grains per photo). The linear-intercept method, conducted to determine grain size, included only grain boundaries and did not count annealing twins as boundaries in the anlaysis. Metallographic sections of the annealed, quasi-statically, and dynamically deformed materials were prepared using standard metallographic techniques for grinding and polishing. The grain structure was revealed by etching in a solution of 50 pct HNO_3 and 50 pct CH_3CO_2H; micrographs were obtained using polarized light. Figure 1 shows the equiaxed grain structure of MONEL 400 as heat-treated to two different grain sizes.

Cylindrical samples, with the compression axis parallel to the wire axis, were electrodischarge machined to dimensions of 5 mm in height and 5 mm in diameter. Samples 9.5 mm in diameter by ~12 mm in length were utilized for mechanical testing nominal grain sizes exceeding 200 μm. Due to the very limited number of grains in the sample cross section for the largest grain size (789 μm), only the data for grain sizes up to 202 μm was utilized in the constitutive-modeling analysis. Quasi-static compression tests were done using an Instron screw-driven test system under a constant strain rate of 0.001 s^{-1}, at temperatures of 77 and 298 K, with $MoSi_2$ lubrication to minimize barreling. Quasi-static testing to large strain values was conducted in increments of ~0.2 true strain, with relubrication and remachining of the sample as required. Dynamic tests at strain rates of 3000 s^{-1} were conducted from 77 to 873 K utilizing a Split–Hopkinson pressure bar.[31] Due to the inherent oscillations in the dynamic stress-strain curves from elastic-wave dispersions and the lack of stress equilibrium in the Hopkinson bar specimens at low strains, the determination of an accurate yield strength at high strain rates is more difficult. Yield values for the Hopkinson bar curves were, therefore, chosen by selecting the flow-stress value at the intersection of the elastic loading line, with a smooth curve back-extrapolated through the plastic-flow data for each curve.

The substructures of MONEL 400 as a function of grain size, in the annealed conditions and following deformation, were examined using transmission electron microscopy

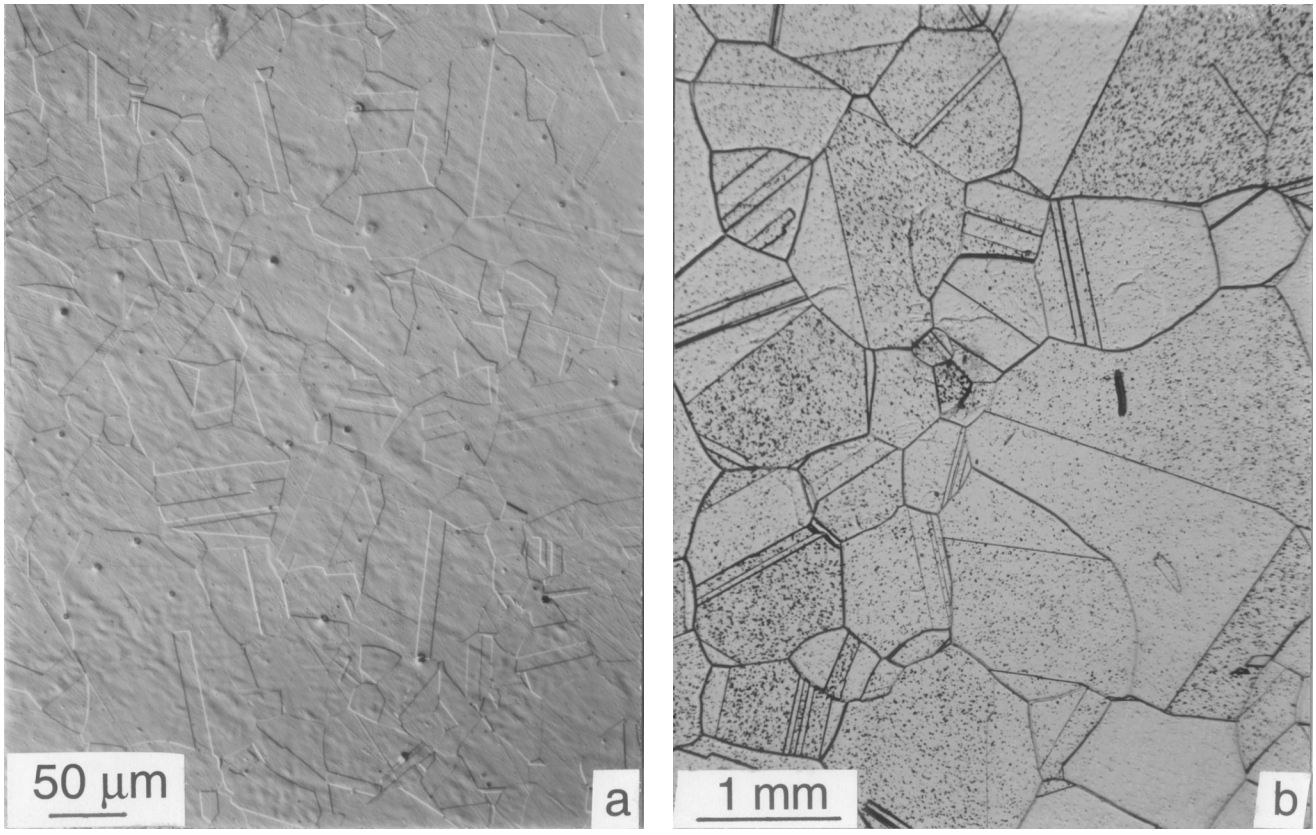

Fig. 1—Optical micrographs of MONEL 400 showing the uniform equiaxed grain structure following heat treatment to obtain grain sizes of (*a*) 51 μm and (*b*) 789 μm.

(TEM). Samples were sectioned using a low-speed diamond saw, and the slices were mechanically thinned. The TEM foils were electrochemically polished in a Struers Tenapol III jet electropolisher to electron transparency, using a solution of 57 pct H_2SO_4 and 43 pct H_2O at 24 °C with an applied voltage of 5 V and a 230 to 250 mA current. Characterization was performed using a PHILLIPS* CM-30 transmission electron microscope equipped with a double-tilt stage, at an accelerating voltage of 300 kV. The bright-field electron micrographs were all taken under a ⟨200⟩ two-beam condition.

*PHILIPS is a trademark of Philips Electronic Instruments Corp., Mahwah, NJ.

III. DESCRIPTION OF MODEL

A. *Mechanical Threshold Stress Model*

The framework and detailed description of the MTS model is given elsewhere,[30,33,34] and a summary of the MTS model has been recently reviewed.[32] Plastic deformation is known to be controlled by interactions of dislocations with obstacles. These interactions are, in general, thermally activated. In the MTS model, the current structure of a material is represented by an internal-state variable, the mechanical threshold, which is defined as the flow stress at 0 K. The mechanical threshold is separated into athermal and thermal components,

$$\hat{\sigma} = \hat{\sigma}_a + \Sigma\hat{\sigma}_t \qquad [2]$$

where the athermal component ($\hat{\sigma}_a$) characterizes the rate-independent interactions of dislocations with long-range barriers such as grain boundaries, dispersoids, or second phases. The sum of the various thermal components ($\hat{\sigma}_t$) characterizes the rate-dependent interactions, which can be overcome with the assistance of thermal activation, of dislocations with various short-range obstacles, such as forest dislocations, interstitials, solutes, the Peierls barrier, *etc.* The flow stress of a constant structure at a given deformation condition is expressed in terms of the mechanical threshold as

$$\frac{\sigma}{\mu} = \frac{\sigma_a}{\mu} + \Sigma S(\dot{\varepsilon}, T)\frac{\hat{\sigma}_t}{\mu_0} \qquad [3]$$

where the athermal component is a function of temperature only through the shear modulus, and the factor S specifies the ratio between the applied stress and the MTS. This factor is smaller than 1 for thermal activation–controlled glide, because the contribution of the thermal activation energy reduces the stress required to force a dislocation past an obstacle. For single-phase cubic materials, we have found that the thermal component can be simplified by the linear summation of a term describing the yield stress ($\hat{\sigma}_i$) and a second term describing theevolution of the dislocation structure ($\hat{\sigma}_\varepsilon$) as a function of temperature, strain rate, and strain. Equation[3] can be rewritten as

$$\frac{\sigma}{\mu} = \frac{\sigma_a}{\mu} + S_i(\dot{\varepsilon}, T)\frac{\hat{\sigma}_i}{\mu_0} + S_\varepsilon(\dot{\varepsilon}, T)\frac{\hat{\sigma}_\varepsilon}{\mu_0} \qquad [4]$$

In the thermally activated glide regime, the interaction kinetics for short-range obstacles are described by an Arrhenius expression of the form

$$\dot{\varepsilon} = \dot{\varepsilon}_0 \exp\left(\frac{-\Delta G}{kT}\right) \qquad [5]$$

The free energy (ΔG) is a function of stress, and a phenomenological relation of the following form has been chosen:[24]

$$\Delta G = g_0\mu\mathbf{b}^3\left[1-\left(\frac{\sigma_t/\mu}{\hat{\sigma}_t/\mu_0}\right)^p\right]^q \qquad [6]$$

Upon rearrangement, we have the following relation between the total applied stress and the mechanical threshold stress ($\hat{\sigma}_t$) at a constant structure:

$$\frac{\sigma_t}{\mu} = \left[1-\left(\frac{kT}{g_0\mu\mathbf{b}^3}\ln\frac{\dot{\varepsilon}_0}{\dot{\varepsilon}}\right)^{1/q}\right]^{1/p}\cdot\frac{\hat{\sigma}_t}{\mu_0} \equiv S_t\cdot\frac{\hat{\sigma}_t}{\mu_0} \qquad [7]$$

The second term on the right-hand side of Eq. [4] describes the rate dependence of the yield stress mainly due to intrinsic barriers, such as the strong Peierls stress in bcc materials at low temperatures or high strain rates; it is, further, assumed that this term does not evolve after yielding. The structure term ($\hat{\sigma}_\varepsilon$) in Eq. [4] evolves with strain due to dislocation accumulation (work hardening) and annihilation (recovery). This structural evolution ($\theta = d\hat{\sigma}_\varepsilon/d\varepsilon$) is represented by a competition between the hardening (θ_0) due to dislocation accumulation and softening ($-\theta_r$) resulting from dynamic recovery (dislocation annihilation and rearrangement), and is written as

$$\theta = \theta_0 - \theta_r(T,\dot{\varepsilon},\hat{\sigma}) \qquad [8]$$

The physical understanding of the work-hardening behavior of polycrystals is still inadequate to unify this complex process and represent it entirely by physically based parameters. Follansbee and Kocks[30] chose the following form to fit their experimental hardening data:

$$\theta = \theta_0\left\{1-\frac{\tanh\left[\alpha\dfrac{\hat{\sigma}_\varepsilon}{\hat{\sigma}_{\varepsilon s}(\dot{\varepsilon},T)}\right]}{\tanh(\alpha)}\right\} \qquad [9]$$

where α, approaching zero, represents a linear variation of the strain-hardening rate with stress (Voce law).[30] The saturation threshold stress ($\hat{\sigma}_{\varepsilon s}$) is a function of temperature and strain rate. Kocks[35] has proposed a description for $\hat{\sigma}_{\varepsilon s}$ that has the same form as that proposed by Haasen[36] for the beginning of dynamic recovery. This relation, in turn, was based on calculations by Schoeck and Seeger[37] of the stress dependence of the activation energy for cross-slip in fcc metals, written as

$$\hat{\sigma}_{\varepsilon s} = \hat{\sigma}_{\varepsilon s0}\left(\frac{\dot{\varepsilon}}{\dot{\varepsilon}_{\varepsilon s0}}\right)^m \qquad [10]$$

where $m = kT/g_{0\varepsilon s}\mu\mathbf{b}^3$, $\dot{\varepsilon}_{\varepsilon s0}$, $g_{0\varepsilon s}$, and $\hat{\sigma}_{\varepsilon s0}$ are constants.

The shear modulus was calculated for fcc materials using the formula

$$\mu = \sqrt{C_{44}\cdot(C_{11}-C_{12})/2} \qquad [11]$$

where C_{ij} are the elastic constants.[38] For simplicity, an empirical equation[39] was used to fit the data to incorporate the temperature dependence of μ, in the form of

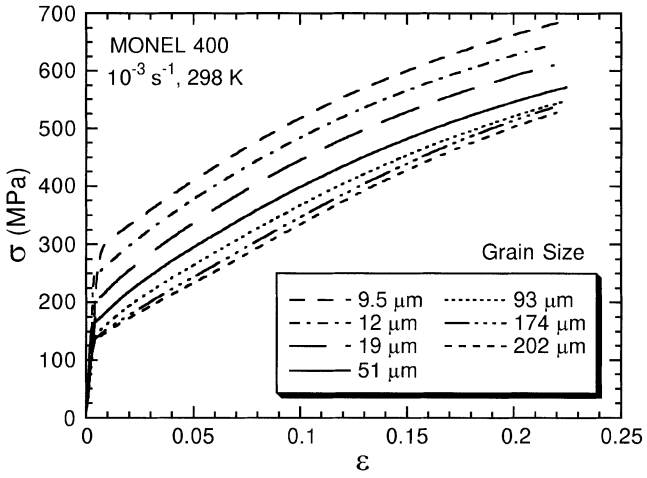

Fig. 2—Plot of the quasi-static stress-strain response of MONEL 400 as a function of grain size.

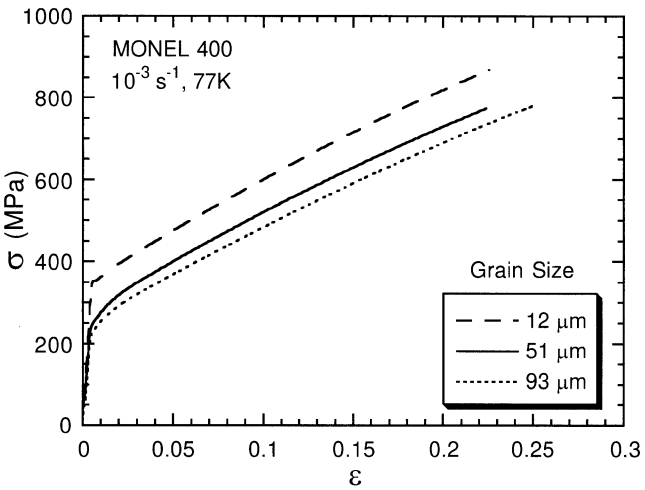

Fig. 3—Plot of the quasi-static stress-strain response of MONEL 400 at 77 K as a function of grain size.

$$\mu = \mu_0 - \frac{D}{\exp\left(\frac{T_0}{T}\right) - 1} \qquad [12]$$

The temperature-dependent shear modulus of Ni was used here for MONEL 400, which is largely Ni-based, using $\mu_0 = 85.09$ GPa, $D = 9.132$ GPa, and $T_0 = 269$ K.

The experimental data at strains less than 0.2 were treated as an isothermal condition for all strain rates, independent of the constitutive model employed.[40] The effect of adiabatic heating at high strain rates was similarly neglected for low strains. In the MTS model, an additional equation is utilized to calculate adiabatic heating effects. The temperature rise for tests at strain rates above 500 s^{-1} can be calculated, assuming a certain percentage (Ψ) of the work of plastic deformation is converted into heat, according to

$$\Delta T = \frac{\Psi}{\rho C_p} \int \sigma \, d\varepsilon \qquad [13]$$

where σ and ε are the true stress and strain, respectively, ρ is the density, and C_p is the heat capacity, which can be written in the form of $A_0 + A_1 \cdot T + A_2/T^2$.[41]

IV. RESULTS

A. *Stress-Strain Response*

The experimentally measured true stress–true strain response of MONEL 400, deformed quasi-statically at 298 and 77 K, is plotted in Figures 2 and 3, respectively. Increasing the grain size from 9.5 to 202 μm is seen to reduce the quasi-static yield strength from 290 to 130 MPa, while having a minimal effect on the work-hardening response of MONEL 400, *i.e.*, the stress-strain curves for all the grain sizes are essentially parallel. The yield strength at 77 K is, similarly, seen to decrease with increasing grain size, although at higher absolute-strength levels from 325 to 225 MPa for grain sizes from 12 to 93 μm. The strain-hardening response at 77 K was also seen to be independent of grain size. Increasing the strain rate from quasi-static to dynamic strain rates is seen to increase yield and overall flow-stress levels, but has no effect on the strong grain-size dependence

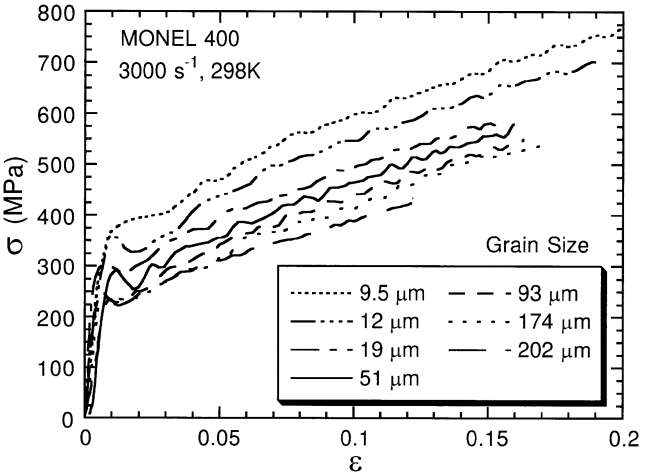

Fig. 4—Plot of the high-strain-rate stress-strain response of MONEL 400 as a function of grain size.

exhibited by this alloy, as shown in Figure 4. The work-hardening rate at high strain rates was, again, seen to remain invariant as a function of grain size.

The yield and flow-stress levels and hardening response exhibited at a given grain size were found to be similar for high-strain-rate and low-temperature deformation, as seen in Figure 5. Low-temperature loading displays a similar rate of strain hardening to that seen under quasi-static loading at true strains of <10 pct. At higher strains, the stress-strain behaviors diverge as the hardening rate decreases, with increasing strain under quasi-static loading at 298 K. This divergence in hardening response is consistent with the suppression of dynamic recovery processes with increasing strain rate or decreased temperature.[42,43] To assess the influence of the total dislocation density and the transition to a greater influence of recovery processes on flow behavior, the stress-strain response of MONEL 400 at two grain sizes was measured to higher strain levels. As shown in Figure 6, the stress-strain behavior for both the 12- and 174-μm grain sizes is seen to exhibit a nearly fixed offset, with no evidence of convergence at higher strain levels.

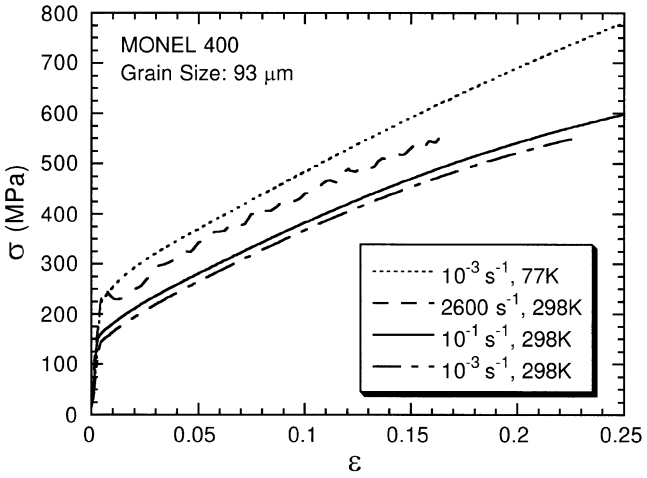

Fig. 5—Stress-strain response of MONEL 400 with a 93-μm grain size as a function of strain rate and temperature.

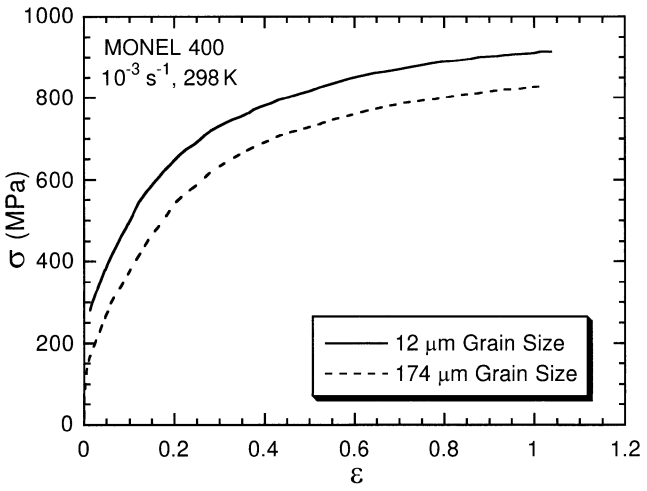

Fig. 6—Plot of the stress-strain response of MONEL 400 at two different grain sizes incrementally reloaded to large strains.

The variation of the quasi-static yield strength with grain size, at room temperature, is shown in Figure 7. The grain sizes are plotted as functions of three different exponents, according to Eq. [1], allowing the correlation for all three exponents to be viewed on a single plot. As has been suggested in the literature, reasonably straight-line dependencies of the yield stress, when plotted as stress *vs* d^n, can be obtained for n values ranging from $n = -1$ to $-1/3$.[1,2,23] The least-squares fitting correlation coefficients were found to be 0.994, 0.992, and 0.984 for the $n = -1$, $-1/2$, and $-1/3$ exponents, respectively. Based solely on the highest correlation, selection of the $n = -1$ exponent is indicated, although the correlation factors for either of the other two exponents are also >0.98. However, the deviations for $n < 1$ are systematic, as indicated by the curvature implied by the points themselves. The influence of strain rate on the grain size–yield stress variation is examined and shown in Figure 8. At strain rates of 0.001 and 3000 s^{-1}, both at 298 K, the slopes of these two correlations, which are a measure of the k_y term in Eq. [1], are seen to be virtually identical. The friction-stress term (σ_0) approximately doubles upon increasing the strain rate by seven orders of magnitude. The

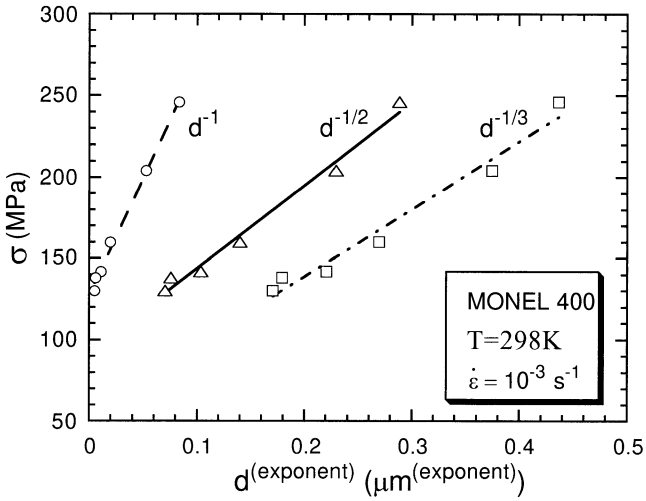

Fig. 7—Hall–Petch plot of MONEL 400 deformed at a quasi-static strain rate as a function of the Hall–Petch coefficient, where the average grain size is in microns.

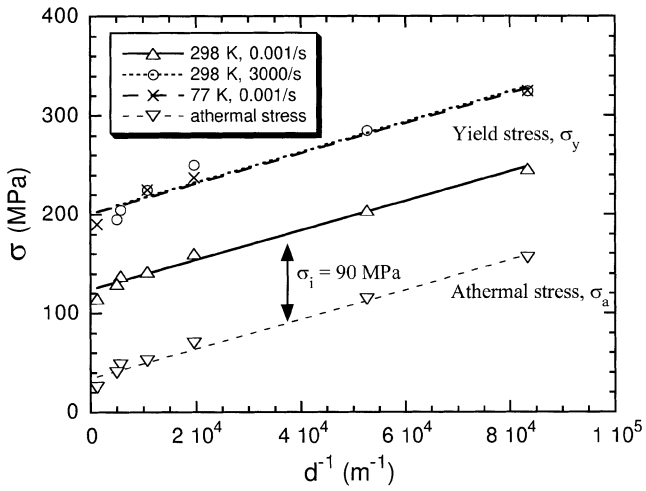

Fig. 8—Hall–Petch plot of yield stresses at 77 and 298 K *vs* d^{-1}, where the grain size is given in units of meters, for MONEL 400 under both quasi-static and dynamic loading conditions.

Table III. Effect of Strain Rate and Temperature on the σ_0 and k_y Terms for MONEL 400

Strain Rate/ Temperature	$d^{-1/2}$		d^{-1}	
	σ_0 (MPa)	k_y (MN/m$^{3/2}$)	σ_0 (MPa)	k_y (MN/m)
10^{-3} s^{-1}/298 K	94.5	0.502	124	0.00150
3000 s^{-1}/298 K	163	0.557	202	0.00153
10^{-3} s^{-1}/77 K	164	0.555	201	0.00152

Hall–Petch plot of the grain size *vs* yield strength at 77 K is also given in Figure 8. The k_y and σ_0 terms for quasi-static deformation at 77 K are almost identical to the same terms for deformation at 3000 s^{-1} and 298 K. The parameters for the Hall–Petch correlations as a function of testing conditions are summarized in Table III.

B. *Deformation Substructure*

The substructure of MONEL 400 was seen to change from an initially low dislocation density after annealing to

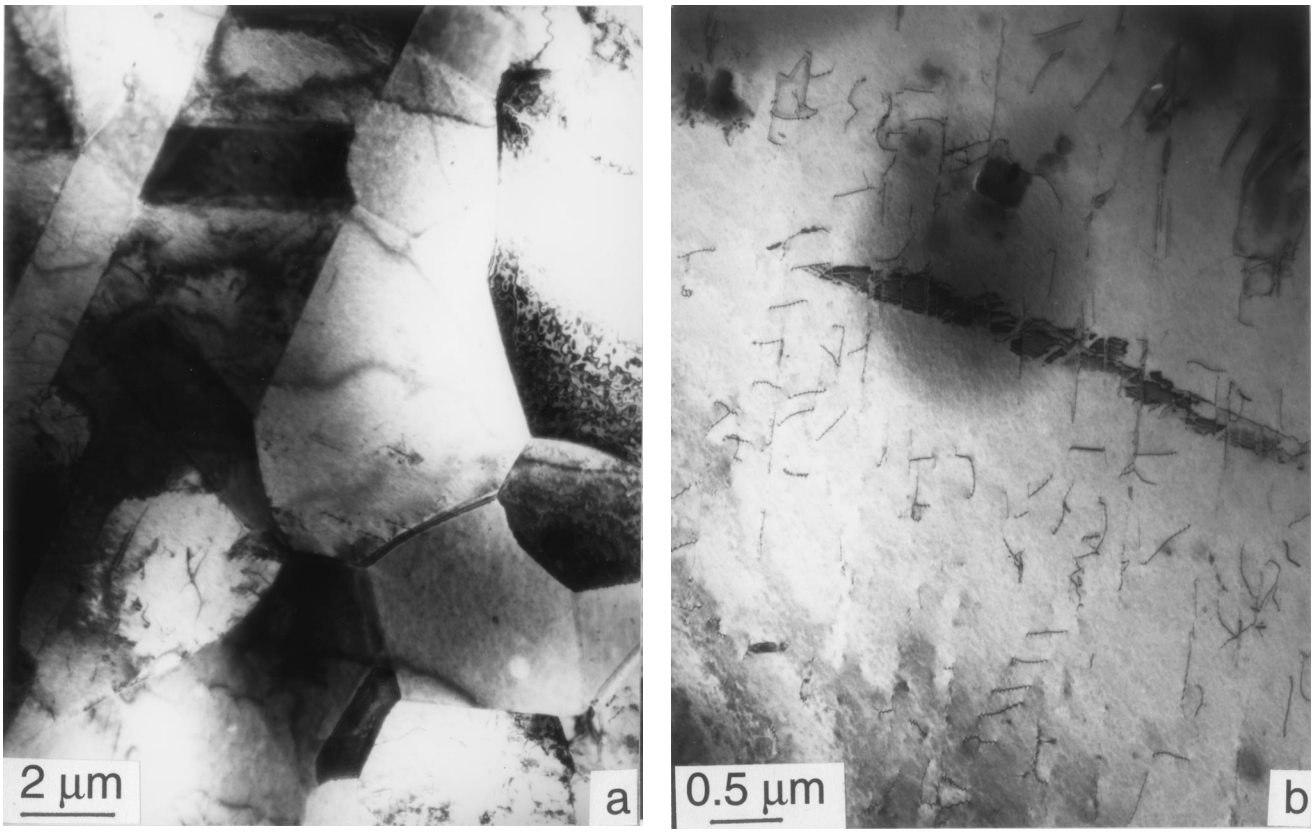

Fig. 9—TEM bright-field micrograph of the as-rolled MONEL 400 showing (*a*) the equiaxed grain structure with low dislocation density and (*b*) the low initial dislocation density in the annealed starting material.

one of dense dislocation structures, the morphology of which was dependent on (1) the starting grain size, (2) the applied strain rate and temperature, and (3) the position within the grain interior or adjacent to the grain boundaries, as in the case of the coarse-grained samples. Figure 9(a) shows the fine, equiaxed grain structure of the as-rolled MONEL 400 specimens. Figure 9(b) reveals the low overall dislocation density resulting from the hot-rolling fabrication. No evidence of residual subgrains or dislocation networks, which might have indicated only partial recovery or incomplete recrystallization, were seen in the starting hot-rolled bar or following any subsequent annealing treatment.

The general substructure evolution in MONEL 400 was seen to consist of dislocation tangles and/or dislocation cells for all temperatures, strain rates, and grain sizes. No evidence of planar or coarse linear-slip arrays were observed in MONEL 400, irrespective of grain size. Increasing the strain rate or decreasing the temperature was seen to alter the cell morphology from that of well-formed cells following quasi-static ambient temperature straining to that of more-loosely connected dislocation tangles under either dynamic loading or testing at 77 K. This observation is consistent with the documented suppression of dynamic recovery processes, with increasing strain rate and/or decreasing temperature resulting from reduced cross-slip and dislocation rearrangement.[42] No deformation twins were observed following any strain-rate/temperature-loading conditions.

The morphology of the substructure was seen to be reasonably uniform within the grains in MONEL 400 at grain sizes below 51 μm, but exhibited pronounced differences between the grain interior and adjacent to the grain boundaries or near grain-boundary triple points at grain sizes greater than or equal to 93 μm. Well-formed dislocation cells were evident in the interior of the 93-μm sample following quasi-static deformation to a true strain of 20 pct (Figure 10(a)), while more-intense planar slip and microbands[44] were found adjacent to many grain boundaries (Figure 10(b)). Elastic and plastic compatibility effects, including local-image stresses, can limit cross-slip and secondary slip in the vicinity of grain boundaries but enhance the degree of primary slip in these regions.[2]

C. *Constitutive Relations*

Description of the constitutive response of MONEL 400 using the MTS model requires systematic identification and model fitting to capture the athermal and thermal contributions to the flow stress, as stated in Eq. [4]. This includes the flow stresses arising from different types of obstacles, including the systematic influence of grain size in the current study. The athermal stress term arises from the interaction of dislocations with long-range barriers such as grain boundaries or distinct reinforcements, as is the case in composites. Experiments over a wide range of temperatures must be conducted to accurately determine the absolute value of the athermal stress component for a material. The stress-strain behavior as a function of grain size, temperature, and strain rate provides a rough estimate of the athermal stress. The yield stress values measured in several low-strain-rate tests

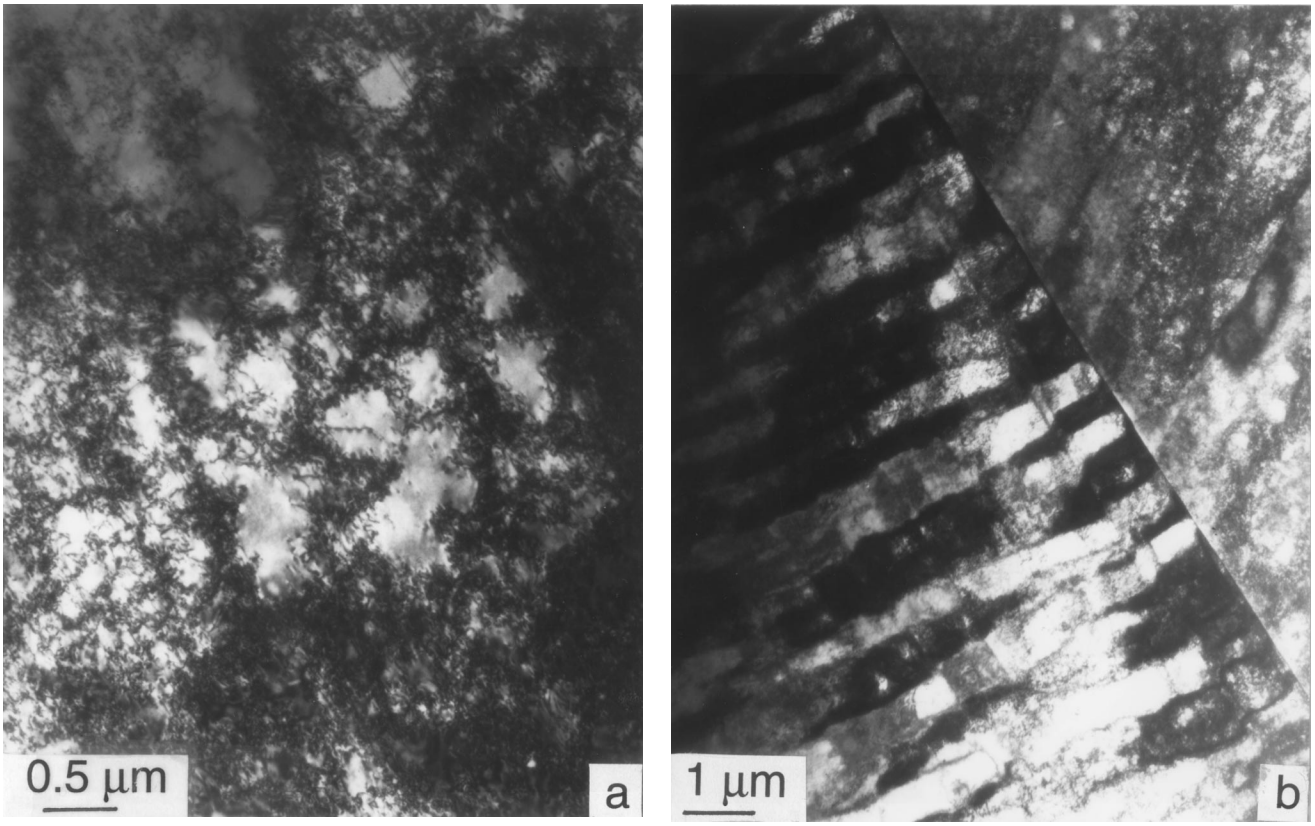

Fig. 10—TEM bright-field micrograph of the 93-μm grain size MONEL 400 following deformation at a strain rate of 10^{-3} s^{-1} at 298 K to a true strain of 20 pct showing (*a*) dislocation cells and (*b*) more intense slip activity and microbands adjoining a grain boundary.

for various grain sizes are plotted in Figure 8. The extrapolation of the fitted curve to very large grain sizes suggests that the yield stress is about 90 MPa, assuming the grain size approaches infinity. At this point, the major contribution to the athermal stress due to the grain size vanishes. As such, this yield stress becomes a reasonable estimate of the maximum thermal component for this material without a grain-size effect. The yield stress of the 51 μm–grain-size MONEL 400 sample, deformed at room temperature and at a low strain rate, was 164 MPa. Taking the difference between the measured yield stress of 164 MPa and the maximum thermal component of 90 MPa gives a value of 74 MPa for the 51-μm MONEL 400 athermal term.

The second term on the right-hand side of Eq. [4] represents the thermal contribution to the yield stress above the athermal contribution. For subsequent analysis, it is assumed that this term does not evolve with strain. In well-annealed materials, the initial dislocation density is sufficiently small that the contribution from the strain-hardening term at very low strains can be neglected. By plotting the yield stress (σ_y) as a function of the normalized activation energy ($kT/\mu\mathbf{b}^3 \cdot \ln(\dot{\varepsilon}_{0i}/\dot{\varepsilon})$), the corresponding parameters which describe the deviation from the mechanical threshold as a function of temperature and strain rate can be determined. The governing Eqs. [4] and [7] can be rearranged as

$$\left(\frac{\sigma_y - \sigma_a}{\mu}\right)^{p_i} = \left(\frac{\hat{\sigma}_i}{\mu_0}\right)^{p_i} - \left(\frac{kT}{g_{0i}\mu\mathbf{b}^3} \ln \frac{\dot{\varepsilon}_{0i}}{\dot{\varepsilon}}\right)^{1/q_i} \cdot \left(\frac{\hat{\sigma}_i}{\mu_0}\right)^{p_i} \qquad [14]$$

where $\dot{\varepsilon}_{0i}$ is an adjustable parameter. An optimum value of $\dot{\varepsilon}_{0i}$ is chosen such that it will collapse all the data at different temperatures and strain rates onto a single curve. The term g_{0i} is the normalized activation energy for this process, in units of $\mu\mathbf{b}^3$, and is also an indication of the sensitivity to changes in temperature and strain rate. The terms p_i and q_i are parameters with the range of $0 < p_i \leq 1$ and $1 \leq q_i \leq 2$, which define the glide-resistance profile in the higher- and lower-activation-energy regions, respectively.[24] The result of this analysis for the 51 μm–grain-size material is shown in Figure 11. Within the range investigated, the yield stress is dependent on temperature and strain rate.

The next step in the development of a complete constitutive description using the MTS model is the evaluation of the strain hardening due to dislocation storage. The constants used in Eqs. [4] and [7] through [10] are determined from the experimental data. For each $\sigma(\varepsilon)$ curve, a corresponding MTS ($\hat{\sigma}(\varepsilon)$) is derived. A series of reloading tests are conducted wherein the material is loaded to a certain deformation state and unloaded; then, this structure is reloaded at different temperatures at a fixed strain rate. The reload yield stress is then plotted according to Eq. [14]. The MTS for the initial structure can then be determined by extrapolating the curve to 0 K. This procedure is repeated for other structure states, namely, to different strains under a given set of test conditions; $\hat{\sigma}(\varepsilon)$ can, thereby, be constructed. A detailed explanation of this process has been described previously.[30] Results of this systematic data-reduction procedure will result in the determination of all the needed constants for the MTS model.

An alternate approach, to shorten this rigorous process, is to use some of the constants derived for OFE (oxygen-

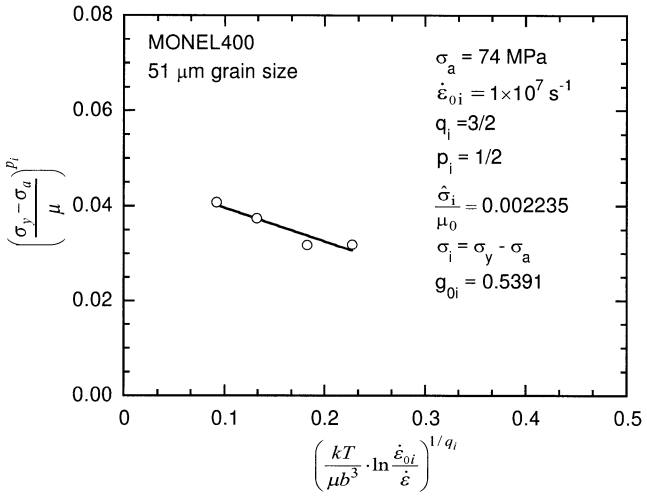

Fig. 11—Yield stresses of the 51-μm grain size material plotted according to Eq. [14].

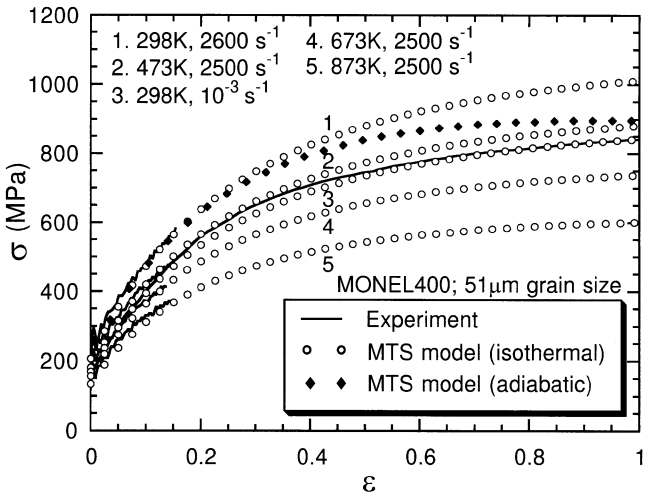

Fig. 12—The stress-strain curves of 51-μm grain size MONEL 400 with the fit to the MTS model, with the open circles representing the best fit to large strains.

free electronic) copper as a first approximation using the previous method, which characterize dislocation interactions with other dislocations, mainly, forest dislocations. The constants in the S_ε factor for copper were $\dot{\varepsilon}_{0\varepsilon} = 10^7\ s^{-1}$, $g_{0\varepsilon} = 1.6$, $p_\varepsilon = 2/3$, and $q_\varepsilon = 1$, $g_{0\varepsilon}$ being the most-critical parameter.[30] Using these values, the calculation of $\hat{\sigma}(\varepsilon)$ from $\sigma(\varepsilon)$ is then done according to Eqs. [4] and [7]. The hardening curve at 0 K was fitted to Eq. [9] to obtain the initial hardening rate and saturation stress of the mechanical threshold. Due to the similarity in the mechanical behavior of OFE-Cu with that measured for MONEL 400, the same relation between θ_0 and $\dot{\varepsilon}$, derived for OFE-Cu in a form of[30]

$$\theta_0 = A + B \cdot \ln \dot{\varepsilon} + C \cdot \sqrt{\dot{\varepsilon}} \qquad [15]$$

was applied to the experimental data here. The saturation stresses at 0 K, fitted for each test condition, are plotted according to Eq. [10] to derive the remaining parameters. The model-fitting results for MONEL 400, with a grain size of 51 μm, are shown in Figure 12 (open circles). An adiabatic calculation was performed for a high-rate room-temperature condition and is plotted in Figure 12 as the filled diamonds. It is seen that the adiabatic effect is minimal at strains less then 0.2. The constants derived for the MTS model for MONEL 400 are summarized in Table IV.

For the purpose of illustration, the grain-size effect in MONEL 400 is accounted for in the MTS model, with the athermal stress component being inversely proportional to the grain diameter (d, measured in meters):

$$\sigma_a = \sigma_0 + \frac{k_y}{d} \qquad [16]$$

From the plot in Figure 8, and assuming that the only factor affecting the yield stress at a constant strain rate and temperature is due to changes in grain size, a value of 90 MPa, which represents the thermal componentis, is subtracted from the yield stresses. The stress-strain curves, with calculated values at 25 °C and $10^{-3}\ s^{-1}$, are plotted in Figure 13. It is not surprising to observe that an excellent agreement is achieved between the fitted curve and the experimental data, since the grain-size effect was derived from this specific testing condition. Figure 14 shows the calculated curves for the dynamic testing condition at 25 °C. The grain-size effect is also well reproduced in this instance, along with the stress levels and the strain-hardening behavior. This plot establishes the applicability of a Hall–Petch relation in describing the grain-size effect on the stress-strain behavior of MONEL 400. In addition, it demonstrates the flexibility of the MTS model to incorporate a new microstructural variable (*i.e.*, a grain-size effect), since the model is based upon the physical processes describing dislocation kinetics.

V. DISCUSSION

A. *Stress-Strain Response*

Grain boundaries have been rationalized to harden metals, because (1) the internal elastic stresses resisting plastic flow are greater in the vicinity of boundaries, and (2) the defect structures are more complex at lower overall strains near grain boundaries than in the grain interior.[2] These defect structures (secondary dislocations, microbands, tangles, *etc.*) increase the local flow stress necessary to penetrate this boundary layer, and, potentially, suppress the operation of dislocation sources at the boundary during subsequent plastic straining. The observations of grain-size effects on the yield and continued flow-stress response of MONEL 400 in this study, as a function of strain rate and temperature, provide (1) points of comparison to previous studies probing experimental loading-parameter effects on grain-size correlations, and (2) some insights into the applicability of various conceptual frameworks to describe grain-size effects on yield and work-hardening behavior.

First, the effect of grain size on the yield strength, as shown in Figures 2 and 4, and the dependence of strain hardening as a function of temperature and strain rate (Figure 5) for a fixed grain size, suggest that contributions from athermal, as well as thermal, effects must be included in any modeling assessment of MONEL 400. The absolute magnitudes and similarities of the Hall–Petch parameters for $d^{-1/2}$, listed in Table III, are consistent with previous values reflecting the effect of loading variables and material alloying on the magnitude of grain-size effects. The overall values of σ_0 and k_y (σ_0 = 94.5 MPa and k_y = 0. 502 MN/

Table IV. Parameters for the MTS model for MONEL 400

Equation	Parameter	Values	Units	Equation	Parameter	Values	Units
12	μ_0	85.09	GPa	4, 7	q_ε	1	—
μ	D	9.132	GPa	S_ε	p_ε	2/3	—
	T_0	269	K	15	A	3363.1	MPa
7, 10	k	1.38×10^{-23}	J/K	θ_0	B	4.7931	$MPa \cdot s^{-1}$
	b	2.49×10^{-10}	m		C	7.4069	$MPa \cdot s^{-1/2}$
4, 16	σ_0	34	MPa	θ	α	1	—
σ_a	k_y	0.0015	MN/m	10	$g_{0\varepsilon S}$	0.37	—
4, 7	σ_i	190.2	MPa	$\hat{\sigma}_{\varepsilon s}$	$\hat{\sigma}_{\varepsilon s0}$	1030	MPa
σ, S_i	$\dot{\varepsilon}_{0i}$	10^7	s^{-1}		$\dot{\varepsilon}_{0\varepsilon s}$	10^7	s^{-1}
	g_{0i}	0.5391	—	13	ρ	8.9	Mg/m^3
	q_i	3/2	—	ΔT	A_0	0.1565	$J/g \cdot K$
	p_i	1/2	—		A_1	0.0007	$J/g \cdot K^2$
4, 7	$\dot{\varepsilon}_{0\varepsilon}$	10^7	s^{-1}		A_2	7059.6	$J \cdot K^3/g$
S_ε	$g_{0\varepsilon}$	1.6	—		Ψ	0.95	—

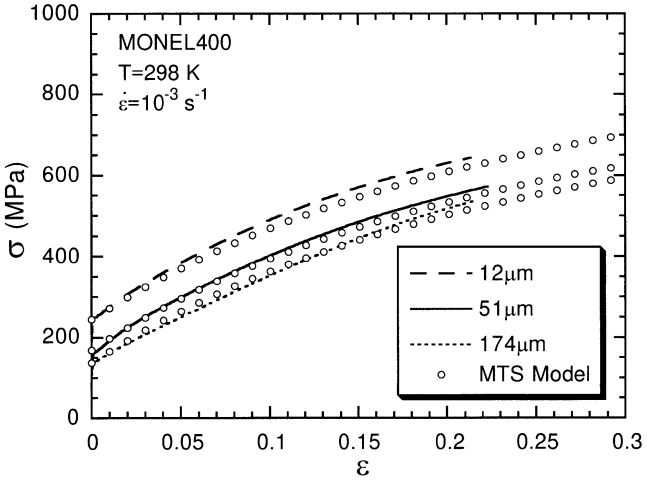

Fig. 13—The stress-strain curves of MONEL 400 compressed at 25 °C at 10^{-3} s^{-1} having various grain sizes, with the fit to the MTS model as the open circles.

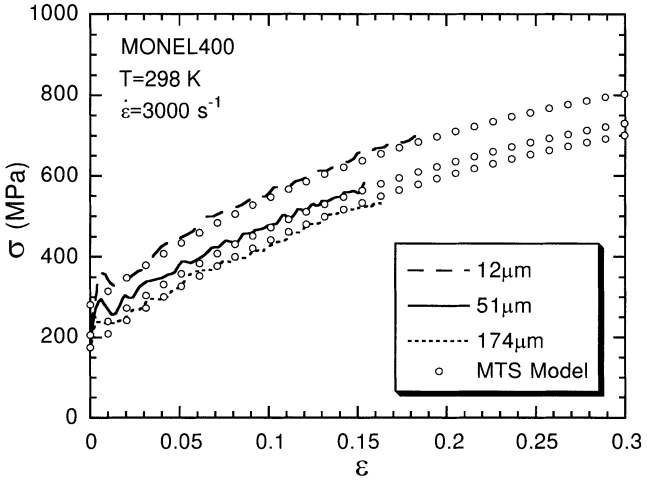

Fig. 14—The stress-strain curves of MONEL 400 deformed at 25 °C under high strain rates having various grain sizes, with the fit to the MTS model as the open circles.

$m^{-3/2}$) determined for room-temperature quasi-static deformation of MONEL 400, assuming a $d^{-1/2}$ correlation, are seen to be considerably higher than those previously reported for the pure constituents in this alloy, *i.e.*, nickel (σ_0 = 34 MPa and k_y = 0.22 $MN/m^{-3/2}$),[1] pure copper (σ_0 = 26 MPa and k_y = 0.12 $MN/m^{-3/2}$),[1] or also for copper[22] (k_y of 0.278 $MN/m^{-3/2}$). A large degree of solid-solution hardening, such as in the current alloy, is thought to increase the values of both σ_0 and k_y due to solute pinning of dislocations, as observed previously for Cu-Zn and Cu-Ni alloys.[20] For a Cu-29Ni-29Zn alloy, where the alloy additions make this alloy somewhat similar, but reversed, in terms of the dominant constituent, the Hall–Petch parameters correlated to $d^{-1/2}$ (σ_0 = 79 MPa and k_y = 0.579 $MN/m^{-3/2}$),[20] are very similar to the values measured here for MONEL 400. The transition in hardening response in MONEL 400 at large strains to a stable stage IV behavior is also consistent with known solute effects on hardening behavior.[45]

Given the superior correlation between d^{-1} for (1) the yield stresses of Monel 400 across the entire range of strain rates and temperatures studied, and (2) the modeling link between d^{-1} grain-size dependency and a sustained grain-size effect to large plastic strains, Table III also contains the Hall–Petch parameters for d^{-1}.

The MONEL 400 data in Figure 7, in particular, the curvatures in the linear fits to various Hall–Petch powers, suggests several points. In pure fcc metals such as Ni[4] and Cu, [22] grain-size studies have shown that the initial yield strength varies linearly with the inverse of the square root of the grain size. However, the Hall–Petch n value for MONEL 400 exhibits the best linear correlation for $n = 1$, rather than the classical $n = 1/2$. This hardening coefficient, in addition to the temperature- and strain rate–dependent work-hardening rates for a fixed grain size and the persistent influence of grain size to large plastic strains, suggests that a direct description of grain-size hardening in Monel 400 based upon a "classical" dislocation-source activation and/or pileup mechanism, consistent with an $n = 1/2$ correlation, is not supported in the current experimental study.

Alternately, a work hardening–based modeling rationale[18] for grain size–dependent strengthening of polycrystals, as previously published in the literature, is consistent with the current experimental observations on MONEL 400. The independence of the work-hardening rate in MONEL 400 on grain size is similar to that displayed by OFE copper.[22] Upon continued deformation, *i.e.*, plastic strains

above 0.3, dense dislocation tangles and arrays in the grain interiors, such as those seen in Figure 10, are expected to exert a dominating influence on the plastic deformation behavior. The substructural evolution differences between the grain interiors and adjacent to grain boundaries in MONEL 400 supports differential defect storage processes which are consistent with the previously published work-hardening modeling arguments.[18] Interestingly, these differences in dislocation morphology were most evident at grain sizes greater than 93 μm, coincident with the curvature exhibited in the Hall–Petch correlations in Figure 7. This alteration in the Hall–Petch power as a function of grain size is similar to the previous experimental results of Hecker *et al.*[46] The differential grain interior–hardening *vs* grain boundary–hardening approach, as derived by Mecking,[18] predicts a d^{-1} dependency which is also consistent with the observed differences in dislocation substructures adjacent to grain boundaries. Conceptually, the composite-region modeling of grain behavior discussed previously[2,18] will not break down, due to an increased dislocation density in the grain interior due to the persistent influence of the grain boundaries on local dislocation motion. However, because this model is derived on athermal differences between the hardening resistance in the grain interior and near boundaries, some influence of both dynamic recovery and total dislocation density on hardening should be important. Once dynamic recovery processes have become important, such as that indicated by the decrease in strain-hardening rates, as shown in Figure 6, at strains >0.6 for MONEL 400, the stress-strain response might be expected to converge at higher strains (or high dislocation densities), which was not observed.

The substructural observations in MONEL 400, when taken with the persistent grain-size effect to large strains, supports the premise that the differential hardening response proposed in the "composite-grain" framework persists. This difference in the grain-size response for MONEL 400 compared to that of pure copper[18] suggests that alloying also plays a strong role in recovery processes relevant to hardening. As saturation is approached in pure copper, differences in dynamic recovery, as a function of grain size, result in convergence of the stress-strain curves for different grain sizes. Conversely, in MONEL 400, the higher initial hardening rates for smaller grain sizes is seen to persist to larger strains. This is consistent with the effect of alloying in MONEL 400 in suppressing dynamic recovery processes. A reduction in recovery processes is consistent with both a transition to stable stage IV hardening in MONEL 400 and the persistent offset in flow-stress levels as a function of grain size to large strains. The current MONEL 400 results suggest that the absolute magnitude of k_y should be significantly increased by alloying in fcc metals and, to a lesser degree, by either temperature or strain rate.

B. *Constitutive Modeling*

In the current study, the MTS model has been shown to be capable of simultaneously capturing the influence of changes in strain rate, temperature, as well as grain size, using a d^{-1} correlation, on the constitutive behavior of MONEL 400. In terms of modeling, the influence of grain size correlates with an alteration in the athermal stress, as previously suggested for grain size.[30] Also consistent with

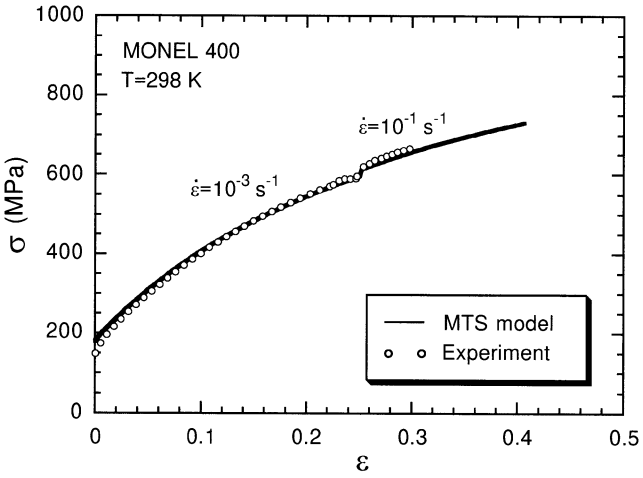

Fig. 15—Calculation of the MTS model and comparison with experimental results of the 51-μm MONEL 400 for a strain rate change from 10^{-3} to 10^{-1} s^{-1} at a strain of 0.25 at 25 °C.

previous studies,[1] the variations in strain rate and temperature of loading were seen to have a small effect on the k_y term. The modeling results for MONEL 400 illustrate that grain-size effects can be readily incorporated into material-constitutive models. However, a robust material-modeling capability first requires an accurate description of yielding and hardening behavior.

It is generally accepted that, at large plastic strains, the stress-strain curves for disordered metals and alloys tend to approach a finite "saturation stress," due to the effects of dynamic recovery processes achieving a balance with dislocation storage.[35] The MTS model uses a differential form, as written in Eq. [9], to fit to the experimental constitutive data. The "ill-defined" integrated strain (from the entire previous deformation history) is, thereby, avoided. The parameter α in Eq. [9] describes the rate at which a material reaches saturation. With the saturation concept and a differential form of hardening law in place, the data obtained under well-controlled conditions is sufficient to derive all the parameters used in Eq. [9].

In addition to a physically based approach to modeling, the balance between work hardening and dynamic recovery processes is a question of path-dependent changes in strain rate and temperature, when taken collectively with athermal stress effects such as grain size. One of the physically realistic attributes encompassed in the MTS model is its capability to calculate flow-stress changes resulting from an arbitrary alteration in strain rate and temperature path. The current structure is characterized by the mechanical threshold. The structural evolution is written as a differential form to eliminate the history effect that is usually associated with substructure, when strain is used as a "state" parameter in the model. Two examples of strain rate–change experiments and the predictions of the MTS model are shown in Figures 15 and 16. In Figure 15, a sample was deformed at 25 °C and 10^{-3} s^{-1} to a strain of 0.25, then the strain rate was changed abruptly to 10^{-1} s^{-1}. The open symbols are the stress-strain response of the material, while the solid line is the calculation from the MTS model. At the point of the strain-rate change in the experiment, where the material structure is constant, the increase in the stress is totally due to the change in

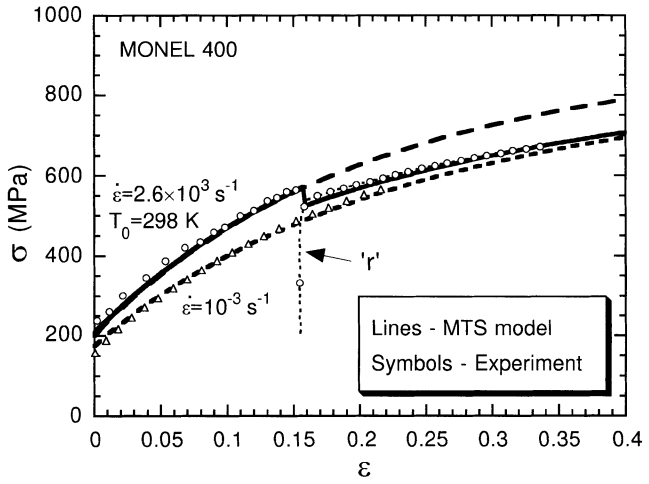

Fig. 16—Calculation of the MTS model and comparison with experimental results of the 51-μm MONEL 400 for a strain rate change from 2600 to 10^{-3} s^{-1} at a strain of 0.165. Curve "r" shows the experimentally measured response of a sample dynamically prestrained at 2600 s^{-1} followed by reloading at 0.001 s^{-1} at 298 K.

deformation condition. The change in strain rate (or temperature) at a given structure results in changes of S_i and S_ε (Eqs. [4] and [8]), as described in the MTS model. These factors determine how much change in stress level accompanies a change in strain rate or temperature in the g_0 term. In this article, g_{0i} was calculated from the plot of the yield stress *vs* normalized activation energy (Figure 11), while $g_{0\varepsilon}$ was assumed to be the same as OFE Cu, which is 1.6.

The agreement between the experiment and prediction, shown in Figure 15, suggests that the assumption of $g_{0\varepsilon}$ being similar to OFE Cu is reasonable. The new structure evolution was then calculated according to Eq. [9], applying an infinitesimal change in strain. The saturation stress used in this equation was updated using Eq. [10] at a new strain rate. Mechanistically, this means that the structure in the material will gradually transition to the structure typical of the yield surface, had the sample been deformed at the new strain rate from the very beginning. Strain-rate jump tests, therefore, provide input data from which to iterate and obtain the activation volume value for the process of glide dislocations interacting with forest dislocations. To obtain the activation volume otherwise would require many reloading tests, as described in the original article by Follansbee and Kocks.[30]

Utilization of strain as a state variable requires that the structure described (*i.e.*, position of the yield surface) will immediately change to that obtained for a sample deformed at a new strain rate or temperature from the very beginning. Accordingly, history or "path-dependent" property effects cannot be readily separated in those models. Another illustration of this point is provided in Figure 16, where a dynamically prestrained sample was reloaded quasi-statically, thereby achieving several orders of magnitude change in strain rate, being loading steps. The long dashed line in this figure represents the calculated stress-strain response under adiabatic conditions to a large strain. The short dashed line is the calculated stress-strain curve under quasi-static conditions, where temperature is constant. The solid line is the MTS model prediction for a sample deformed adiabatically at a high strain rate to a strain of 0.165. After the strain-rate change, the calculation is resumed at 25 °C at a strain rate of 10^{-3} s^{-1}; this is illustrated by the remainder of the solid line in Figure 16. The open circles represent the experimental stress-strain behavior for the sample subjected to the previously defined strain-rate path change, while the open circles, labeled "r," represent the mechanical response when the sample prestrained at 2600 s^{-1} is reloaded quasi-statically. The agreement between the MTS model prediction and the experimental data demonstrates, additionally, the ability of the MTS model to satisfactorily capture path-dependent phenomena and grain-size dependency simultaneously.

VI. SUMMARY AND CONCLUSIONS

Based on a study of the influence of grain size on the strain-rate dependence of the flow stress for MONEL 400, the following conclusions can be drawn.

1. The influence of grain size on the mechanical behavior of MONEL 400 is shown to be due to an athermal d^{-1} contribution to the flow stress of MONEL 400, which is persistent to large plastic strains. The persistent influence of grain size to large strains is inconsistent with previous $d^{-1/2}$ pileup grain-size modeling in the literature, which predicts convergence at large strains. Substructural evolution differences between the grain interiors and adjacent to grain boundaries supports differential defect storage processes which are consistent with previously published work-hardening d^{-1} modeling arguments for grain size–dependent strengthening in polycrystals.
2. The strain rate and temperature sensitivity of the flow stress and the insensitivity of the strain-hardening rate indicate that thermally activated dislocation slip is the rate-controlling mechanism for deformation in MONEL 400 in the temperature regime from 77 to 873 K.
3. The MTS model overall is shown to provide robust fitting results to both yield and large strain constitutive response, simultaneously, as a function of temperature, strain rate, and grain size using a d^{-1} correlation, as well as to satisfactorily address the experimentally observed transients due to strain-rate or temperature-path dependency.

ACKNOWLEDGMENTS

The authors acknowledge the contributions of R.W. Carpenter for performing the dynamic tests and M.F. Lopez for performing the quasi-static tests and optical metallography. The authors thank Inco Alloys International Inc. (Huntington, WV) for providing the MONEL 400 used in this study. The authors acknowledge U.F. Kocks for critically reviewing this manuscript and Sig Hecker for helpful discussions. GTG and KSV would like to express their appreciation to the Institute of Mechanics of Materials at the University of California at San Diego for providing partial funding and organizational support for this work. GTG and SRC acknowledge that portions of this research were performed under the auspices of the United States Department of Energy.

REFERENCES

1. E.O. Hall: *Yield Point Phenomena in Metals and Alloys*, Plenum Press, New York, NY, 1970, p. 296.
2. J.P. Hirth: *Metall. Trans.*, 1972, vol. 3, pp. 3047-67.
3. R.W. Armstrong: *Metall. Trans.*, 1970, vol. 1, pp. 1169-76.
4. T. Narutani and J. Takamura: *Acta Metall. Mater.*, 1991, vol. 39, pp. 2037-49.
5. M. Dollar and A.W. Thompson: *Acta Metall.*, 1987, vol. 35, pp. 227-35.
6. A.M. Omar and A.R. Entwisle: *Mater. Sci. Eng.*, 1969–1970, vol. 5, pp. 263-70.
7. Z.C. Szkopiak: *Mater. Sci. Eng.*, 1972, vol. 9, pp. 7-13.
8. D. Kuhlmann-Wilsdorf: *Mater. Sci. Eng.*, 1989, vol. A113, pp. 1-41.
9. E.O. Hall: *Proc. Phys. Soc.*, 1951, vol. B64, p. 747.
10. N.J. Petch: *J. Iron. Steel Inst.*, 1953, vol. 174, p. 25.
11. G.T. Gray III, J.C. Williams, and A.W. Thompson: *Metall. Trans. A*, 1983, vol. 14A, pp. 421-33.
12. A.W. Thompson and W.A. Backofen: *Acta Metall.*, 1971, vol. 19, pp. 597-606.
13. A.W. Thompson: *Acta Metall.*, 1975, vol. 23, pp. 1337-42.
14. W.M. Baldwin: *Acta Metall.*, 1958, vol. 6, p. 139.
15. U.F. Kooks: *Acta Metall.*, 1959, vol. 7, p. 131.
16. H. Conrad: *Acta Metall.*, 1963, vol. 11, p. 75.
17. E. Anderson, L. King, and J. Spreadborough: *Trans. AIME*, 1968, vol. 242, p. 115.
18. H. Mecking: in *Deformation of Polycrystals: Mechanisms and Microstructures*, N. Hansen, A. Horsewell, T. Leffers, and H. Lilholt, eds., Riso National Laboratory, Roskilde, Denmark, 1981, pp. 73-86.
19. J.D. Embury: *Strengthening by Dislocation Substructures*, Applied Science Publishers Ltd., Barking, Essex, United Kingdom, 1971, pp. 331-402.
20. W. Koster and M.O. Speidel: *Z. Metallkd.*, 1965, vol. 56, pp. 585-98.
21. J. Harding: *Acta Metall.*, 1969, vol. 17, pp. 949-58.
22. W.H. Gourdin and D.H. Lassila: *Acta Metall. Mater.*, 1991 vol. 39, pp. 2337-48.
23. U.F. Kocks: *Metall. Trans.*, 1970, vol. 1, pp. 1121-43.
24. U.F. Kocks, A.S. Argon, and M.F. Ashby: *Progr. Mater. Sci.*, 1975, vol. 19, p. 1.
25. G.R. Johnson and W.H. Cook: *Proc. 7th Int. Symp. on Ballistics*, American Defense Preparation Organization (ADPA), The Hague, Netherlands, 1983, pp. 541-47.
26. F.J. Zerilli and R.W. Armstrong: *J. Appl. Phys.*, 1987, vol. 61, pp. 1816-25.
27. T.J. Holmquist and G.R. Johnson: *3rd Int. Conf. on Mechanical and Physical Behavior of Materials under Dynamic Loading*, Strasbourg, France, *J. Phys.*, 1991, vol. 1, pp. C3-853-C3-860.
28. R.W. Armstrong, F.J. Zerilli, W.H. Holt, and J.W. Mock: *High-Pressure Science and Technology-1993*, Colorado, Springs, CO, 1993, S.C. Schmidt, J.W. Shaner, G.A. Samara, and M. Ross, eds., American Institute of Physics, New York, NY, 1994, vol. 2, pp. 1001-04.
29. F.J. Zerilli and R.W. Armstrong: *High-Pressure Science and Technology—1993*, Colorado Springs, CO, 1993, S.C. Schmidt, J.W. Shaner, G.A. Samara, and M. Ross, eds., American Institute of Physics, New York, NY, 1994, vol. 2, pp. 989-92.
30. P.S. Follansbee and U.F. Kocks: *Acta Metall.*, 1988, vol. 36, pp. 81-93.
31. P.S. Follansbee: *High Strain Rate Compression Testing-The Hopkinson Bar*, 9th Mechanical Testing ed., ASM, Metals Park, OH, 1985, vol. 8, pp 198-203.
32. S.R. Chen and G.T. Gray III: *Metall. Mater. Trans. A*, 1996, vol. 27A, pp. 2994-3006.
33. P.S. Follansbee, J.C. Huang, and G.T. Gray: *Acta Metall. Mater.*, 1990, vol. 38, pp. 1241-54.
34. P.S. Follansbee and G.T. Gray: *Metall. Trans. A*, 1989, vol. 20A, pp. 863-74.
35. U.F. Kocks: *J. Eng. Mater. Technol.*, 1976, vol. 98, pp. 76-85.
36. P. Hassen: *Phil. Mag.*, 1958, vol. 3, pp. 384-418.
37. G. Schoeck and A. Seeger: *Defects in Crystalline Solids*, Physical Society, London, 1955.
38. G. Simmons and H. Wang: *Single Crystal Elastic Constants and Calculated Aggregate Properties: A Handbook Second Edition*, The MIT Press, Boston, MA, 1991.
39. Y.P. Varnish: *Phys. Rev. B*, 1970, vol. 2, pp. 3952-58.
40. S.R. Chen and G.T. Gray: *Tungsten and Refractory Metals 2*, A. Bose and R.J. Dowding, eds., Metal Powder Industries Federation, Princeton, NJ, 1995, pp. 489-98.
41. D.R. Stull and G.C. Stinke: *Thermodynamic Properties of the Elements*, D.R. Stull and G.C. Stinke, eds., American Chemical Society, Washington, D.C., 1956.
42. G.T. Gray III: *Deformation Substructures Induced by High Rate Deformation*, TMS-AIME, Warrendale, PA, 1991, pp. 145-58.
43. U.F. Kocks: *Strain Hardening and 'Strain-Rate Hardening,'* ASTM STP 765, ASTM, Philadelphia, PA, 1982, pp. 121-38.
44. J.C. Huang and G.T. Gray: *Acta Metall.*, 1989, vol. 37, pp. 3335-47.
45. D.A. Hughes and W.D. Nix: *Metall. Trans. A*, 1988, vol. 19A, pp. 3013-24.
46. S.S. Hecker, M.G. Stout, and D.T. Eash: *Experiments on Plastic Deformation at Finite Strains*, Stanford University, Stanford, CA, 1982, pp. 162-205.